rijksuniversiteit groningen

faculteit Wiskunde en Natuurwetenschappen

Energy transfer in light-harvesting complexes

Bacheloronderzoek Wiskunde\Natuurkunde

Juni 2012

Student: G. Vos

Eerste Begeleider: T.L.C. Jansen

Tweede Begeleider: B. Carpentieri

Abstract

Light harvesting complexes have naturally developed structures such that energy transfer processes on the ultrafast timescale can occur. It is of large practical interest to be able to predict the transport properties of chain-like molecular structures. This thesis provides a relatively simple model to describe the mechanics behind such processes. Specifically the model was decoupled into a set of classical coordinates and quantum mechanical two-level systems. Numerical simulations have been used to investigate time-evolution of such systems for varying parameters, and from the results some conditions for maximizing the transport rate were found.

Contents

1 Introduction

With the recent advent of 2D infrared and electronic microscopy it is possible to follow processes on the femtosecond time scale. An example of such a process is the resonant energy transport between nearby molecules, where an excited molecule can pass its excitation on to another molecule. These types of processes are interesting since they allows chain-like structures to pass on an excitation from the first site to other sites. If a reaction center is located at the end of the chain where the excitation can be converted into another form of energy. Because of the rapid nature of the individual transportations, the total harvesting of the excitation can take place in the order of picoseconds. Therefore the excitation can be harvested before it has had the chance to relax to the groundstate or otherwise dissipate to its surroundings, this causes these transfer processes to have extremely high efficiencies, close to 100%.

The most common example of such a process is the photosynthesis process in plants. A natural light harvesting system is depicted below in figure 1.

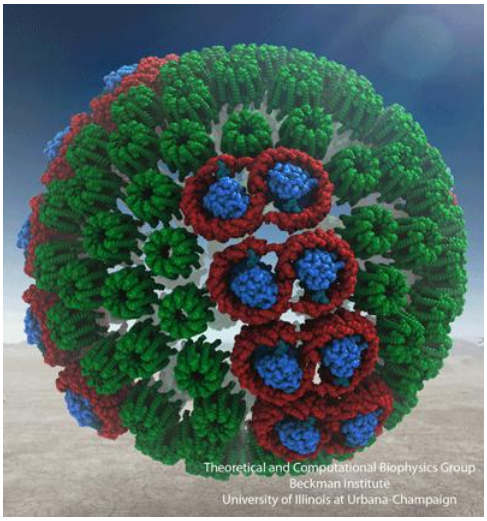

Figure 1: This digital model represents a natural light harvesting system. The green structures represent LH1 chromophores, structures that can absorb light. The red elements represent LH2 chromophores and the blue structures are reaction centers which can convert an excitation into a different form of energy [2].

It is of common interest to be able to understand these processes, since such transport properties are highly desired in solar cells and nano devices. Therefore many phenomenological models have been proposed, as seen in for example [4], [5].

An electronically excited state, implies that an electron has left its orbital to occupy a higher level one. Therefore an abstract concept as an excitation

can be made more concrete by considering it to be a bound electron-hole pair. This can essentially be modeled as a single particle, which is called an exciton. Therefore the problem is changed from modelling the energy transfer process, to modelling the dynamics of this exciton. This exciton will be allowed to be able to fully delocalize over the chain.

To perfectly evaluate such a structure, the state of the molecules and its electrons has to be considered. This is not practical due to massive amount of degrees of freedom involved. Instead the Born-Oppenheimer approximation is applied. This approximation states that it is reasonable to separate the wave function into a product function of the nuclear coordinates and electronic coordinates. To simplify matters more in molecular dynamics it is typical that these nuclear coordinates are evaluated using classical dynamics instead of quantum dynamics.

To explicitly state the main questions involved: based on the previous statements a model will be proposed, this model will be simulated numerically, stability conditions will be found such that the result should be reliable. Most results were found for a dimer (i.e. a chain consisting of two sites) and some results for a polymer chain of 25 sites.

2 Theory

The full model is build up from two subsystems. One models the electronic coordinates of the system and will be called the quantum subsystem. The other system models the larger scale properties of the individual molecule, as mentioned before this system can reasonably be described using classical dynamics. Therefore that system will be called the classical subsystem.

To model the whole chain of molecules, a quantum mechanical two-level system and a classical mass-spring system was associated with every site of the chain. The resulting two-level systems are electronically coupled via dipole-dipole interactions. This allows the exciton to delocalize over the sites of the chain. The classical coordinates will be coupled to a Gaussian heat bath, this will allow the classical particles to absorb or dissipate energy from or to the bath. Both of these subsystem will be coupled together such that both subsystems can influence each other, this will create a feedback system. The full model is displayed pictorially in figure 2.

The set-up of the experiment is as follows: a chain of N sites is considered. It is assumed that a reaction center is located at the N^{th} site of the chain, this reaction traps a large fraction of the population that reaches this site. This transfer process is simulated until practically the entire population has diminished. A measure of the amount of time this took (the harvesting time) is calculated at the end.

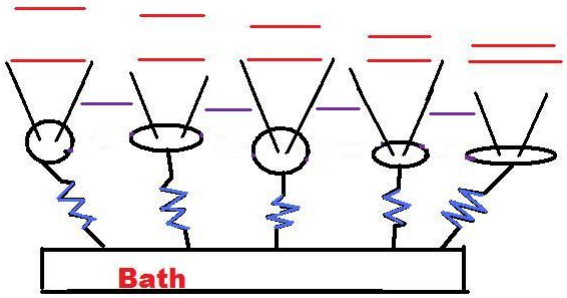

Figure 2: The basic model. The deformed spheres designate excited molecules, the blue lines designate the springs attached to the classical system and the purple lines designate the inter site coupling.

2.1 Quantum subsystem

It is assumed that the evaluated chain has a positive energy gradient towards the trap. Therefore it is assumed that the energy level of the excited state decreases linearly with the sites. The increment with which the energy decreases with every site is called the bias, which is denoted by Δ. The sites are coupled via a coupling constant J. To designate the state of the Frenkel exciton it is necessary to specify a basis. The site basis was chosen, where designates $|n>$ a state vector denoting full localization on the n^{th} site. In this basis the Hamiltonian has the following form:

$$H_{quantum} = \begin{pmatrix} (n-1)\Delta & J & \frac{J}{8} & \frac{J}{27} & \dots & \frac{J}{(n-1)^3} \\ J & (n-2)\Delta & J & \frac{J}{8} & \dots & \\ \frac{J}{8} & J & (n-3)\Delta & J & & \\ \vdots & & & & \ddots & \\ \frac{J}{(n-1)^3} & & & \dots & J & 0 \end{pmatrix}. \quad (1)$$

This is called the Frenkel excitonic Hamiltonian [4]. As can be seen the energy of the site with the lowest energy is set to zero. Actual relaxation of the energy to the ground state is not incorporated since it is at first a very slow process compared to the trapping process and secondly since it can very easily be calculated post rem by multiplying the total population by a exponential function of time, since it would effect all sites equally.

The coupling factor J_{nm} and its dependence on $\frac{1}{n^3}$ has the following origin. In molecular aggregates, excitations can move from molecule to molecule via the Förster resonance energy transfer mechanism (FRET). In which the relaxation of an excited molecule incites an excitation in one of the other molecules in the polymer/aggregate. Dexter resonance energy transfer (DRET) which involves the exchange of electrons requires significant overlap of the wave functions and

typically the intermolecular distance is great enough to neglect it, i.e. in Fenna-Matthews-Olson complexes (FMO) the minimal intermolecular distance is 11 nm [7]. The coupling strength of FRET is due to the dipole-dipole coupling between nearby molecules, therefore the intersite coupling strength J is proportional to $\sim \frac{1}{r^3}$, DRET on the other hand has a coupling strength proportional to $\sim \frac{1}{r^5}$ [1].

2.1.1 Theoretical solution to the double site problem

To test whether Matlab could accurately calculate the dynamics of the quantum system a simple dimer was evaluated analytically and compared to numerical experiments. To find the time development of the quantum system, the time-dependent Schrödinger equation needs to be solved,

$$i\hbar\dot{\psi} = H\psi. \tag{2}$$

The Hamiltonian of the double site problem has the following form

$$H = \begin{pmatrix} \Delta & J \\ J & 0 \end{pmatrix}. \tag{3}$$

Where J is the coupling between sites and Δ is the energy difference between sites. The eigenvalues and eigenvectors are determined by the characteristic polynomial

$$\lambda^2 + \Delta\lambda - J^2 = 0. \tag{4}$$

Solving the characteristic polynomial reveals the following eigenvalues:

$$e_{1/2} = -\frac{\Delta}{2} \pm \frac{\sqrt{\Delta^2 + 4J^2}}{2}. \tag{5}$$

From this, the eigenvector equations can be solved and the following eigenvectors were found:

$$v_1 = \begin{pmatrix} 1 \\ \frac{e_1}{J} \end{pmatrix}, \tag{6}$$

$$v_2 = \begin{pmatrix} 1 \\ \frac{e_2}{J} \end{pmatrix}. \tag{7}$$

The time evolution operator of the system is evaluated by first diagonalizing the Hamiltonian using the spectral decomposition:

$$H = \frac{J}{e_2 - e_1} \begin{pmatrix} 1 & 1 \\ \frac{e_1}{J} & \frac{e_2}{J} \end{pmatrix} \begin{pmatrix} e_1 & 0 \\ 0 & e_2 \end{pmatrix} \begin{pmatrix} \frac{e_2}{J} & -1 \\ -\frac{e_1}{J} & 1 \end{pmatrix}. \tag{8}$$

The time evolution operator then becomes,

$$\begin{aligned} T = e^{-\frac{i}{\hbar}Ht} &= \frac{J}{e_2 - e_1} \begin{pmatrix} 1 & 1 \\ \frac{e_1}{J} & \frac{e_2}{J} \end{pmatrix} \begin{pmatrix} e^{-\frac{i}{\hbar}e_1 t} & 0 \\ 0 & e^{-\frac{i}{\hbar}e_2 t} \end{pmatrix} \begin{pmatrix} \frac{e_2}{J} & -1 \\ -\frac{e_1}{J} & 1 \end{pmatrix} \\ &= \begin{pmatrix} \frac{1}{e_2 - e_1}(e_2 e^{-\frac{i}{\hbar}e_1 t} - e_1 e^{-\frac{i}{\hbar}e_2 t}) & \dots \\ \frac{J}{(e_2 - e_1)}(\frac{e_1 e_2}{J^2} e^{-\frac{i}{\hbar}e_1 t} - e^{-\frac{i}{\hbar}e_2 t}) & \dots \end{pmatrix}. \end{aligned} \tag{9}$$

The elements other than those in the first column are irrelevant as it is always assumed that we start with an initial state fully localized at the first site. The other elements will just get multiplied by zero. Since in the basis that was used, the initial state vector is of the form:

$$\psi_0 = \begin{pmatrix} 1 \\ 0 \end{pmatrix}. \tag{10}$$

Therefore the population at the high energy site as a function of time is

$$\begin{aligned} P_s &= \left(\frac{1}{e_2 - e_1}\right)^2 (e_2 e^{-\frac{i}{\hbar}e_1 t} - e_1 e^{-\frac{i}{\hbar}e_2 t})^\dagger (e_2 e^{-\frac{i}{\hbar}e_1 t} - e_1 e^{-\frac{i}{\hbar}e_2 t}) \\ &= \left(\frac{1}{e_2 - e_1}\right)^2 \left(e_1^2 + e_2^2 + e_1 e_2 \left(e^{\frac{i}{\hbar}(e_1 - e_2)t}\right) + e_1 e_2 \left(e^{\frac{i}{\hbar}(e_2 - e_1)t}\right)\right), \end{aligned} \tag{11}$$

from which it can be noted that the maximum localization relative to the equilibrium is proportional to the product of the eigenvalues, the frequency at which the population oscillates between the two sites is proportional to the distance between the two eigenvalues. When subtracting the two found eigenvalues and denoting the frequency by ω, the following expression for ω can be found:

$$\omega^2 = \frac{1}{\hbar^2}(\Delta^2 + 4J^2). \tag{12}$$

On a different note, the equilibrium position shifts upwards as Δ increases. Hence resonant energy transfer is visible in this system as the fraction of the population that shifts to a neighboring site increases as $\Delta \longrightarrow 0$. This of course does not reveal any underlying physics, rather it is a sign of a well-designed model.

2.2 Classical subsystem

To model the energy fluctuation and environmental response of the larger scale system a classical coordinate is kept track of. This coordinate measures the amount of energy the system has. The Born-Oppenheimer approximation justifies the separation the molecular coordinates from the electronical coordinates. To be more true to nature these molecular coordinates have to be evaluated quantum mechanically, this is an extremely non-trivial affair and therefore an approach typical to molecular dynamics is applied, namely to keep track of the energy of the molecule as a classical point particle in a potential well. The position dependence of the potential is chosen to be quadratic (i.e. a harmonic oscillator) for a more generic potential see [4]. We want the system to be able to lose energy through dissipation to the heatbath and be able to absorb energy from the bath. To model the dissipation, a friction term is added to the equation of motion where γ is a friction factor which represents the coupling strength to the bath. Furthermore it is assumed that nothing is known about the bath,s so

we model the absorption of energy as a Gaussian distributed fluctuating force with a very short correlation time

$$m\ddot{x} = -kx - m\gamma\dot{x} + F^{heat}, \tag{13}$$

where k represents a spring constant, γ is a friction coefficient and F^{heat} is a random Langevin force. The Langevin force is modeled as being Gaussian distributed with mean zero and a correlation function:

$$< F^{heat}(0)F^{heat}(t) >= 2m\gamma k_b T\delta(t). \tag{14}$$

The Langevin force increases as γ increases since it is a measure of how much contact the oscillator has with the bath.With this force included the system is no longer isolated from the outside world. The Langevin force models the systems interaction with the heat bath. It is clear that energy is not internally conserved; rather the energy of the greater system which is not modeled in full detail is conserved.

2.3 Coupled system

To allow the two subsystems to interact with each other, they are coupled together to create a feedback system. The classical system is coupled to the quantum system by adding a coupling Hamiltonian to the Frenkel exitonic Hamiltonian:

$$H = H_{\text{Frenkel}} + H_{\text{coupling}} \tag{15}$$

Where H_{Frenkel} is equal to (1) and H_{coupling} is defined as

$$H_{nm}^{\text{coupling}} = -Cx_n(t)\delta_{nm}. \tag{16}$$

Here C is the coupling coefficient with unit $(\text{cm nm})^{-1}$ and x_n is the coordinate of the harmonic oscillator coupled to the n^{th} site. The time dependence of the Hamiltonian is provided by the coupling Hamiltonian. The coupled quantum Hamiltonian is now of the form

$$H_{nm} = (-(n-1)\Delta - Cx_n)\,|n >< n| + J_{nm}|n >< m|. \tag{17}$$

Where the individual elements of J_{nm} are defined as:

$$J_{nm} = \begin{cases} 0 & \text{if} \quad n = m \\ \frac{J}{|n-m|^3} & \text{if} \quad n \neq m \end{cases}$$

To couple the quantum subsystem to the classical subsystem a force term is added. This force term is linearly dependant on the localisation of the exciton on the n^{th} site:

$$m\ddot{x} = -kx - m\gamma\dot{x} + F^{heat} + hcC|< n|\psi >|^2. \tag{18}$$

In the last term on the right hand side, h is the Planck constant and c is the speed of light.

An interesting effect caused by the feedback of the quantum system is the property referred to as the Stokes shift. The observation that the emission spectrum of a system is somewhat shifted relative to the absorption spectrum is referred to as the Stokes shift and the coupled quantum-classical system has a similar property. In the absence of the quantum system the classical system can be seen as a simple quadratic potential well. If the feedback is activated and the exciton is largely populated on a specific site, a constant force is added to the harmonic oscillator coupled to that site. This force will cause the potential well to shift, therefore the minimum will shift to a new position, which the particle will relax into. This new position is coupled back to the quantum system lowering the energy of that site. The magnitude of this effect is determined in the following way. The force applied to the n^{th} harmonic oscillator when fully localized on the n^{th} site is equal to hcC, hence the potential well will be shifted to

$$V(x) = \frac{1}{2}kx^2 - hcCx. \tag{19}$$

Which has a new minimum located at $x = \frac{hcC}{k}$. Since parameters will be chosen such that the harmonic oscillator will be overdamped (see the section; Parameters and justifications) the coordinate will quickly shift to this new equilibrium when fed back into the Hamiltonian then by (16) this leads to a shift in the n^{th} diagonal element of magnitude equal to

$$\Delta\omega = -C^2\frac{hc}{k}. \tag{20}$$

It is hypothesized that this shift can cause a ripple effect that causes the population to quickly cascade through the system, as demonstrated in figure 3.

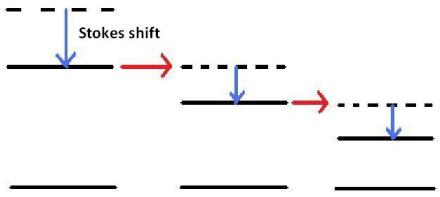

Figure 3: The Stokes shift (equation 20) causes the energy levels to drop. It is believed to be able to cause the exciton to quickly pass through the system.

3 Methods

3.1 Integration of the classical system

To integrate the individual classical particles, the Verlet integration scheme was applied [11]. The Verlet algorithm can be used for system that are time reversible. Of course because of the random Langevin force, this equation is irreversible for larger timescales, but locally (i.e. for small timesteps) the equation is reversible. The Verlet equation is described as follows

$$x(t+\Delta t) = 2x(t) + \frac{F}{m}(\Delta t)^2 - x(t-\Delta t). \tag{21}$$

It is derived in the following way. From the Taylor polynomial, it is known that

$$x(t+\Delta t) = x(t) + v(t)\Delta t + \frac{F}{2m}(\Delta t)^2 + \frac{1}{6}\frac{d^3x}{dt^3}(\Delta t)^3 + O((\Delta t)^4). \tag{22}$$

Exploiting the time symmetry of Newtonian dynamics, the following can also be written down

$$x(t-\Delta t) = x(t) - v(t)\Delta t + \frac{F^{heat}}{2m}(\Delta t)^2 - \frac{1}{6}\frac{d^3x}{dt^3}(\Delta t)^3 + O((\Delta t)^4). \tag{23}$$

Adding these last two expressions together yields

$$x(t+\Delta t) + x(t-\Delta t) = 2x(t) + \frac{F}{m}(\Delta t)^2 + O((\Delta t)^4), \tag{24}$$

from which the above explicit algorithm directly follows.

To demonstrate the convergence of this algorithm the following test problem was integrated

$$m\ddot{x} = -kx, \tag{25}$$

$$x(0) = 1, \tag{26}$$

$$\dot{x}(0) = 0. \tag{27}$$

which is the equation of motion of a free harmonic oscillator. The analytical solution is

$$x(t) = cos\left(\sqrt{\frac{k}{m}}t\right). \tag{28}$$

Table (1) below shows the result of numerical integration versus the analytical solution. From table (1) it can be seen that the local truncation error converges with 4^{th} order and the global error converges with second order.

The friction term in the equation of motion is problematic. The friction force is proportional to the velocity, but the velocity term was canceled out in the

$\Delta t(ps)$	local error (x$10^{-6}(nm)$)	Q	global error	Q
0.001	0.00000625		0.000023	
0.002	0.000100	16.00	0.000093	4.00
0.005	0.00391	39.06	0.00058	6.25
0.01	0.0625	16.00	0.0023	4.00
0.02	0.997	15.99	0.0093	4.00

Table 1: Q is the convergence factor between successive errors. The global error was taken over an interval of 50 time units.

Verlet scheme. The usual way of handling this is the Verlet-velocity algorithm which has the following form.

$$x(t+\Delta t) = x(t) + v(t)\Delta t + a(t)\frac{(\Delta t)^2}{2}, \tag{29}$$

$$v(t+\frac{\Delta t}{2}) = v(t) + \frac{1}{2}a(t)\Delta t, \tag{30}$$

$$a(t+\Delta t) = -\frac{k}{m}x(t) - \gamma v(t+\frac{\Delta t}{2}) + \frac{F^{heat}}{m} - \frac{Chc}{m}|<n|\psi>|^2, \tag{31}$$

$$v(t+\Delta t) = v(t+\frac{\Delta t}{2}) + \frac{1}{2}a(t+\Delta t)\Delta t. \tag{32}$$

This algorithm uses the same approach as the Verlet method, but also explicitly calculates the velocity at every step [11]. The stability suffers for it though, the Verlet method has a local truncation error of the order $(\Delta t)^4$; the Verlet velocity method on the other hand has a local truncation error of the order $(\Delta t)^2$. Approximating the velocity at every timestep and using it for more than just the friction term seems needlessly expensive, since the velocity is exclusively used in the friction term. The following alternatives are considered.

3.1.1 Backwards finite difference-Verlet

An alternative way to handle the problem is to use the backwards finite difference method to estimate the velocity at each timestep and use that in the friction term. In which case the difference equation has the following form

$$x(t+1) = 2x(t) - x(t-1) - \left(\frac{k}{m}x(t) + \frac{F}{m} - \frac{Chc}{m}|<n|\psi>|^2\right)(\Delta t)^2 + \gamma\left(x(t) - x(t-1)\right)\Delta t. \tag{33}$$

3.1.2 Central difference-Verlet

The central finite difference method for approximating a derivative converges faster than the backwards finite difference method. When implemented in the Verlet scheme, the following implicit method is found

$$x(t+1) = 2x(t) - x(t-1) - \left(\frac{k}{m} x(t) + \frac{F}{m} - \frac{Chc}{m} | < n | \psi > |^2 \right) (\Delta t)^2 + \frac{1}{2} \gamma \left(x(t+1) - x(t-1) \right) \Delta t, \tag{34}$$

which can be rewritten to the following explicit method

$$x(t+\Delta t) = \frac{2x(t) - x(t-1) - \left(\frac{k}{m} x(t) + \frac{F}{m} - \frac{Chc}{m} | < n | \psi > |^2 \right) (\Delta t)^2 + \frac{1}{2} \gamma x(t-1)}{1 + \frac{1}{2} \gamma \Delta t}. \tag{35}$$

3.2 Truncation errors

3.2.1 Backwards finite difference

For the backwards finite difference-Verlet method, the local truncation error can easily be found using Taylor polynomials. It was already shown that the standard Verlet method has a local error of order $(\Delta t)^4$. The backwards finite difference method itself has a local error of the order Δt

$$\begin{aligned} x(t+1) = 2x(t) - x(t-1) - \frac{1}{m} \left[kx(t) + F^{heat} - Chc | < n | \psi > |^2 \right] (\Delta t)^2 \\ + \gamma \left[\frac{(x(t) - x(t-1))}{\Delta t} + O(\Delta t) \right] (\Delta t)^2 + O((\Delta t)^4). \end{aligned}$$

From which it can be seen that the local truncation error is of the order $(\Delta t)^3$. The next step is to find the global truncation error. The error in the nth timestep is defined as ϵ_n. Then

$$\begin{aligned} \epsilon_{n+1} &= 2\epsilon_n - \epsilon_{n-1} - \left(\frac{k}{m} (\Delta t)^2 + \gamma \Delta t \right) \epsilon_n + \gamma \Delta t \epsilon_{n-1} + O((\Delta t)^3) \\ &= \left(2 - \frac{k}{m} (\Delta t)^2 - \gamma \Delta t \right) \epsilon_n - (1 - \gamma \Delta t) \epsilon_{n-1} + O((\Delta t)^3). \end{aligned} \tag{36}$$

The next thing that will be done is to show that certain choices of timesteps exist such that the propagation error will not diverge. Therefore from now on it will be assumed that at the points t and $(t - \Delta t)$ the the local error is negligible, which is reasonable since if it would not be then the solution was stable to begin with. First note that the error of the next timestep depends linearly on the previous timesteps. So it can be written in the following form:

$$\epsilon_{n+1} = \begin{pmatrix} 2 - \frac{k}{m} (\Delta t)^2 - \gamma \Delta t & 1 - \gamma \Delta t \end{pmatrix} \begin{pmatrix} \epsilon_n \\ \epsilon_{n-1} \end{pmatrix}, \tag{37}$$

apply the Cauchy-Schwarz inequality

$$(x, y) \leq ||x||||y|| \tag{38}$$

to find

$$\epsilon_{n+1} \leq M\sqrt{\epsilon_n^2 + \epsilon_{n-1}^2}, \tag{39}$$

where

$$M \equiv \sqrt{\left(2 - \frac{k}{m}(\Delta t)^2 - \gamma\Delta t\right)^2 + (1 - \gamma\Delta t)^2}. \tag{40}$$

Assume $r = \max(\epsilon_n, \epsilon_{n-1})$ by considering the previous errors as the legs of a right angled triangle and applying the pythagorean theorem it can be seen that an upper bound can be found by setting both previous errors equal to r:

$$\sqrt{\epsilon_n^2 + \epsilon_{n-1}^2} \leq r\sqrt{2}, \tag{41}$$

from which we find

$$\epsilon_{n+1} \leq Mr\sqrt{2}. \tag{42}$$

From the definition of r it follows that the propagated error is stable if $M^2 \leq \frac{1}{2}$. To make the calculation easier, note that

$$M^2 \leq (2 - \gamma\Delta t)^2 + (\gamma\Delta t - 1)^2 = 2\gamma^2(\Delta t)^2 - 6\gamma\Delta t + 5. \tag{43}$$

Solving the inequality for Δt yields

$$2\gamma^2(\Delta t)^2 - 6\gamma\Delta t + \frac{9}{2} \leq 0 \tag{44}$$

$$\Delta t = \frac{3}{2\gamma}. \tag{45}$$

Hence it has been shown that for given parameters there exists a reasonable timestep (since γ is rather large see the section 'Parameters and justifications') such that the global error does not diverge greatly. Note that due to the large amounts of successive inequalities and bounds that were used that in reality this system will be stable in an interval around $\frac{3}{2\gamma}$ rather than in a single point. Also mind that in the limit case $dt \longrightarrow 0$ the local error will propagate, but for reasonable time intervals the result should still not diverge greatly. The reason for this is that the local error is still of magnitude $(\Delta t)^3$, therefore it would take large amounts of timesteps before the error starts to become large relative to the exact solution. This in practice is of course not an issue since it is not practical to have both and extremely small timestep and an extremely large time interval.

To find the global truncation error, reinstate the local truncation error as in equation (37). Assuming a Δt was chosen so that the error behaves as described in (45), then

$$\epsilon_{n+1} \leq r + O((\Delta t)^3). \tag{46}$$

By construction $\epsilon_0 = \epsilon_1 = 0$ hence through complete induction it follows that

$$\epsilon_n \leq nO((\Delta t)^3). \tag{47}$$

Because of the equidistant roster, the error at the time $T = n\Delta t$ can be described as

$$\text{error}(x(T)) \leq \frac{T}{\Delta t} O((\Delta t)^3) \simeq O((\Delta t)^2). \tag{48}$$

Hence the finite difference-Verlet method has a global error of order $(\Delta t)^2$. [12]

This was tested by letting the algorithm calculate a simple dampened harmonic oscillator as a test problem,

$$m\ddot{x} = -kx - m\gamma\dot{x}. \tag{49}$$

The analytical solution for initial conditions $x(0) = 0 \quad \dot{x}(0) = 1$ of an overdamped system is,

$$x(t) = \frac{2}{\sqrt{\gamma^2 - \frac{k}{m}}} \left(e^{-\frac{\gamma}{2} + \frac{1}{2}\sqrt{\gamma^2 - \frac{k}{m}}} - e^{-\frac{\gamma}{2} - \frac{1}{2}\sqrt{\gamma^2 - \frac{k}{m}}} \right). \tag{50}$$

Letting the finite difference-Verlet method integrate this equation of motion, and taking the maximum value of the difference between the approximated solution and the analytical solution for different timesteps yields the following table.

$\Delta t(ps)$	global error (nm)$(*10^{-3})$	Q
0.001	0.0028	
0.002	0.0011	3.9786
0.005	0.00674	6.1503
0.01	0.2625	3.8946
0.02	0.9957	3.7935

Table 2: Q is the factor between successive errors, γ was scaled in every experiment to fit (Δt) as in (45).

It can be seen that the global error decreases with order $(\Delta t)^2$, as the theory would suggest. In figure 4 the dramatic consequences of the inappropriate choice of the timestep are visible.

3.2.2 Central difference method

Using a similar analysis as for the backwards finite difference method, first write the error in the next timestep as a linear combination of the error in the previous two steps

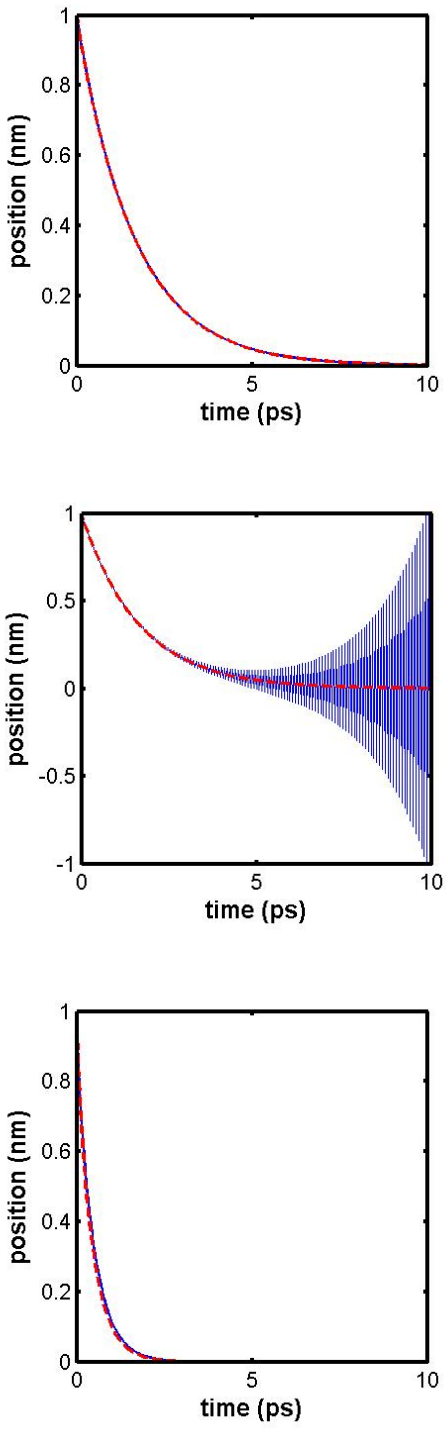

Figure 4: These graphs display the integration of the test problem described in eqn. (49), using the Verlet-BFD scheme. The first two use $\gamma = 50\text{ps}^{-1}$ and respectively $\Delta t = 0.01$ps and $\Delta t = 0.04$ ps, the last image uses $\gamma = 16\text{ps}^{-1}$ and $\Delta t = 0.04$ ps. k is equal to 30 u ps^{-2} in all three cases. It can be seen that the choice of parameters can have large consequences.

$$\epsilon_{n+1} = \frac{2 - \frac{k}{m}(\Delta t)^2}{1 + \frac{1}{2}\gamma\Delta t}\epsilon_n + \frac{\frac{1}{2}\gamma\Delta t - 1}{1 + \frac{1}{2}\gamma\Delta t}\epsilon_{n-1} + O((\Delta t)^4). \tag{51}$$

The same upper bound as before can be constructed

$$\epsilon_{n+1} \leq \sqrt{2}M\max(\epsilon_n, \epsilon_{n-1}). \tag{52}$$

where

$$M^2 = \frac{1}{(1 + \frac{1}{2}\gamma\Delta t)^2}\left(\left(2 - \frac{k}{m}(\Delta t)^2\right)^2 + \left(\frac{1}{2}\gamma\Delta t - 1\right)^2\right). \tag{53}$$

Just as before a sufficient but not necessary condition for prevention of error propagation is revealed:

$$M^2 \leq \frac{1}{2}.$$

Unfortunately this equation seemingly cannot be reduced further. By plotting eqn. (53) as seen in figure 5, it can be seen that the timesteps for which is sure that the error will not propagate are too large to evaluate physically relevant parameters.

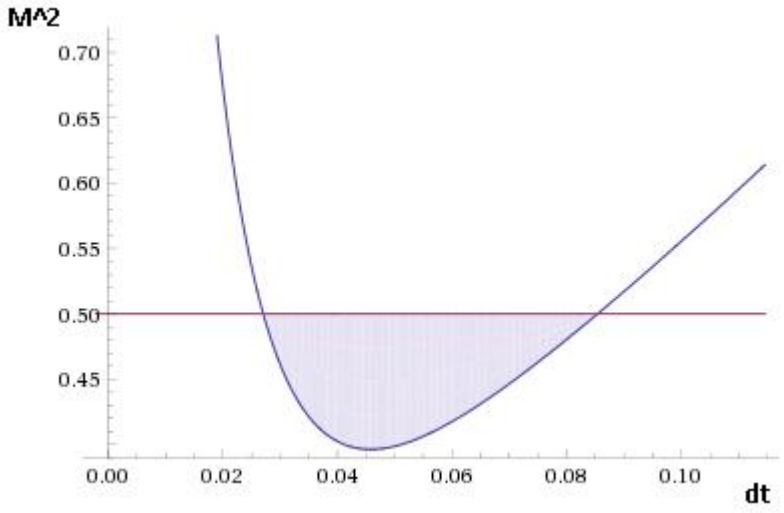

Figure 5: A graphical depiction of the region where (53) holds. The blue line represents M^2 as a function of Δt the shaded area depicts the region were M^2 is smaller than or equal to 0.5.

3.3 Analysis of the quantum system

The quantum system is evaluated using Numerical Integration of the Schrödinger Equation (NISE) [10]. The basic idea is that the Hamiltonian though a function of time does not vary rapidly on the timescale of the integration step size, therefore the Hamiltonian is taken to be constant over the duration of single integration step. The justificaction of this approach is due to the Frank-Condon principle, which states that the fluctuation of the electronic coordinates of a system is generally significantly faster than the fluctuation in the nuclear coordinates [1]. In Matlab [18] the *expm()* function was used to calculate the time evolution operator of the Hamiltonian. Using this, the state at the next timestep was determined

$$\psi(x, t + \Delta t) = e^{-\frac{i}{\hbar} H \Delta t} \psi(x, t). \tag{54}$$

To check whether the numerical solution matches the theoretical solution found in the subsection 'Theoretical solution to the double-site problem', the following specific situation was evaluated

$$\Delta = 3,$$
$$J = 2.$$

In which case the eigenvalues reduce to

$$e_1 = -4,$$
$$e_2 = 1.$$

And the eigenvectors are equal to

$$v_1 = \begin{pmatrix} -\frac{1}{2} \\ 1 \end{pmatrix}, \tag{55}$$

$$v_2 = \begin{pmatrix} 1 \\ \frac{1}{2} \end{pmatrix}. \tag{56}$$

The time-evolution operator is now easily found:

$$U = e^{-\frac{i}{\hbar} H t} = \begin{pmatrix} \frac{1}{5} e^{4iq} + \frac{4}{5} e^{-iq} & \dots \\ -\frac{2}{5} e^{4iq} + \frac{2}{5} e^{-iq} & \dots \end{pmatrix} \tag{57}$$

where

$$q \equiv \frac{t}{\hbar}.$$

Assuming an initial state that is fully localized at the site with the highest energy, the population amplitude squared as a function of time can be found to be

$$A = |\frac{1}{5} \left[\cos(4q) + 4\cos(q) + i(\sin(4q) - 4\sin(q))\right]|^2$$

$$= (1/25) \left[17 + 8\cos(4q)\cos(q) - 8\sin(4q)\sin(q)\right],$$

which overlaps completely with the found numerical solution as can be seen in figure (6).

3.4 Complexity

All the mentioned methods have been implemented in Matlab [18]. The complexity of the used method is dominated by the step at which the time-evolution operator is constructed. Matlab's built-in *expm*() command is used to approximate the matrix exponential. Matlab uses the scaling and squaring algorithm introduced by Higham in [13] to calculate the matrix exponent. This algorithm is based on the following property of exponents

$$e^A = \left(e^{\left(\frac{A}{2^n}\right)}\right)^{2^n}. \tag{58}$$

This method first scales the matrix by dividing it by a power of 2 until its norm is sufficiently small. The resulting matrix exponent is approximated with Padé approximants, the result is then repeatedly squared to counteract the initial divisions. The amount of matrix multiplications required is

$$n = \pi_m + log_2(||A||/\theta_m), \tag{59}$$

where m is the order of the Padé approximants and π_m is the amount of matrix multiplications required to compute the approximant. The second term signifies the amount of times the result has to be squared to find the final result. From reference [13], the values for π_m are

m	3	5	7	9	13
π_m	2	3	4	5	6

Table 3: number of matrix multiplications necessary to evaluate a Padé approximant of order m.

The boundary of the convergence region of a m^{th} order Padé approximant is designated $\theta(m)$. These values are given in the following table. For n sites

m	3	5	7	9	13
θ_m	0.01496	0.254	0.950	2.098	5.372

Table 4: The boundary within the scaled norm of H should fall.

$$||H||_\infty = (n-1)\Delta + \sum_{i=1}^{n-1} \frac{J}{i^3}. \tag{60}$$

For example in the case $n = 25$, $\Delta = 400cm^{-1}$ and $J = 600cm^{-1}$, the required amount of matrix multiplications is 17, since the infinity norm in this case is

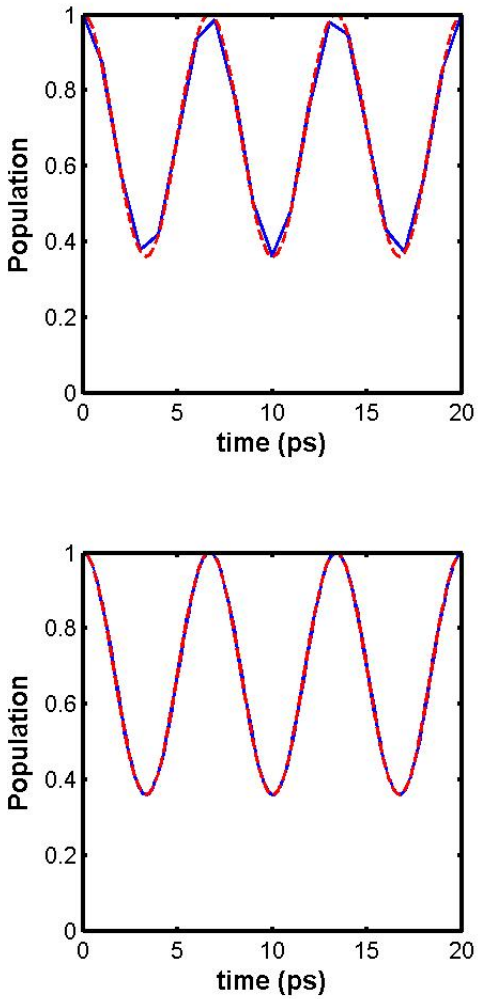

Figure 6: The graphs display the population at the high energy site of a dimer as a function of time, in the case of zero intersystem coupling and no harvesting. The red dashed lines are the theoretical values the blue solid lines represent the numerical values. The first image uses $\Delta t = 0.1$ ps the second uses $\Delta t = 0.01$ ps.

$$||H||_\infty = 9600 + \sum_{i=1}^{24} \frac{600}{i^3} \simeq 9600 + 1.2 * 600 = 10320. \tag{61}$$

The origin of the factor 1.2 is that it is roughly equal to the Riemann zeta function evaluated at 3. Successively dividing by 2 yields

$$\frac{10320}{2^{11}} = 5.039,$$

$$\theta_9 < 5.039 < \theta_{13}.$$

The most efficient approximation is a 13^{th} order Padé approximant which requires 6 matrix multiplications, bringing the total to $11 + 6 = 17$ matrix multiplications. For a dimer with Δ ranging from 0 to 500 it can similarly be seen that the computation requires either 12 or 13 matrix multiplications.

Since the evaluation of the $expm()$ function requires square matrix multiplications and the dimension of the Hamiltonian is equal to the amount of sites, the complexity rises as the amount of sites cubed. To check this,

it was timed how long it took to compute the time evolution operator of a Frenkel excitonic hamiltonian (1) of n sites. The results are displayed in figure 7.

As can be seen from the bottom graph in figure 7, the cube root of the computational time increases linearly with the amount of sites, or equivalently the computational time increases with n^3.

3.5 Parameters and justifications

The model from the previous section demands the selection of parameters described in table 5.

Parameters	
m	mass of the molecule in u
k	spring constant of the molecule in $\frac{\text{u}}{\text{ps}^2}$
γ	friction coefficient in ps^{-1}
T	temperature of the surroundings in K
J	the coupling between sites in cm^{-1}
Variables	
Δ	the energy difference between sites in cm^{-1}
C	the coupling of the classical system to the quantum system in $(\text{cm nm})^{-1}$

Table 5: The necessary parameters and variables that are used in the model.

To help choose physically relevant parameters, we want to satisfy the following few relations. First, to suppress the dependence on one parameter the mass-spring system was chosen to be overdamped, which occurs when

$$\gamma^2 > 4\frac{k}{m}. \tag{62}$$

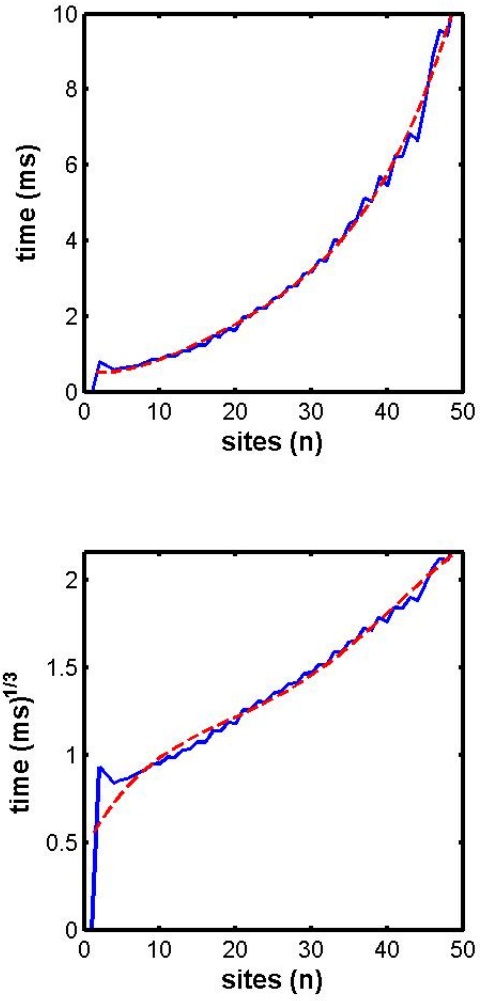

Figure 7: The computational time in milliseconds required to construct the Frenkel exitonic Hamiltonian (1) and the time evolution operator set out against against the amount of sites n. The result was averaged over 500 iterations. The time was found using Matlab's tic toc commands. The blue solid line are the found values, the red dashed line represent a fourth order least squares approximation through the blue line. The graph on the bottom is the same as graph on the top only the amount of sites is set out in a cubic manner. From this it can be seen that for small amount of sites the computational time increases roughly quadratically but for larger amounts of sites the increase is cubic.

Furthermore, the coupled system needs to have a reasonable correlation time

$$\tau = \frac{m\gamma}{k}, \tag{63}$$

$$0.1\text{ps} < \tau < 1\text{ps}. \tag{64}$$

The correlation time is a property of the classical coordinate that is somewhat similar to a relaxation time, in the overdampened system the correlation time is measure of the amount of time it takes for the classical coordinate to settle back into the bottom of its potential well after it has been displaced from its equilibrium position. This in turn limits Δt since the timestep has to be significantly smaller than the correlation time. The application of the NISE method depends on the assumption that the Hamiltonian does not wildly fluctuate over the course of a single timestep. It was also shown that $\Delta t \sim \frac{3}{2\gamma}$ Putting another restriction on γ.

One of the main questions of this thesis to answer is what the effect of the Stokes shift on the harvesting time of the population. The Stokes shift is a property that was mentioned in the section labeled coupling above,

$$\Delta\omega = -C^2\frac{hc}{k}. \tag{65}$$

The following parameters were chosen

m	1
γ	137
k	274
T	300
Δt	0.01
J	600

The reasoning is as follows. The typical displacement of the classical coordinate is of the order of 0.1 nm from the above analysis it follows that we want a (Δt) that is not greater than 0.01 ps. In this this case the global truncation error is typically not greater than 10% of the displacement. To keep the Stokes shift somewhat in check the mass is set to 1 u, a somewhat specific value but hydrogen can act as a chromophore. By choosing a correlation time $\tau = 0.5$ ps, k can be expressed in terms of γ by (64)

$$k = 2\gamma. \tag{66}$$

Substituting this in M^2 from (40) and evaluating the inequality, we have

$$M^2 = (2 - 2\gamma * 0.01^2 - \gamma * 0.01)^2 + (1 - 0.01 * \gamma)^2 \leq 0.5. \tag{67}$$

The lowest value of γ that can surely be used according to the above inequality is $\gamma = 137$ ps^{-1}, which implies $k = 274$ u ps^{-2}. The value $J = 600$ cm^{-1} was chosen because this value is typically associated to pseudoisocyanine (PIC) aggregates, which are synthetic light harvesting systems [4].

3.6 Scripts

The way of answering the posed questions has been to numerically simulate the dynamics of the coupled system a large amount of times and averaging over all the found trajectories. As was already shown instead of immediately developing a script that would simulate the coupled system, as intermediate steps separate scripts were made that simulated the quantum system and N classical systems separately. Following this, a larger script was created that followed the path demonstrated in 8.

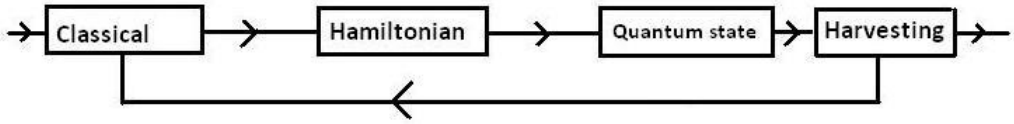

Figure 8: Flowchart describing the integration process.

Hence first all the N classical systems were propagated by one timestep. From the new positions the diagonal elements of the Hamiltonian are reconstructed. The following step is the most time consuming one, namely to propagate the state of the quantum system by constructing the time evolution operator and using it to operate on the state function, then a large fraction of the population located at Nth site is transferred away from the system. This new state is then fed back into the classical equation of motion and the next timestep is again calculated. This process is repeated until sufficiently large amount of timesteps have passed such that the total excitation has almost fully been harvested. When this has occurred M times, where M is the amount of calculated trajectories the average total population as a function of time is calculated. The harvesting time is defined as

$$\tau_h = \int_0^\infty \psi^\dagger \psi \; dt. \tag{68}$$

Expecting an integral over an infinite time interval is of course unreasonable, but if the decay rate and/or the total amount of timesteps is great enough a reasonable approximation can be made by integrating up to the final time. To do this the trapezoidal rule was applied

$$\int_0^\infty < \psi | \psi > dt \simeq -\frac{1}{2}\psi(0)^\dagger\psi(0) - \frac{1}{2}\psi(t_f)^\dagger\psi(t_f) + \sum_{n=0}^{t_f} \psi(n)^\dagger\psi(n), \tag{69}$$

where t_f is the final time [15]. The reason the trapezoidal rule was chosen is that the inherent randomness of the system is still clearly visible in the final

result even when averaged over 500 trajectories. The error of the trapezoidal rule is not large compared to the random deviations, hence any other integration rules (e.g. Simpson's rule) would just be unnecessarily costly.

As an intermittent step the coupled system without trapping and with the list of parameters as seen in table 6 was run.

m	5
k	1111.7
γ	50
T	300
Δ	500
J	100
Δt	0.01

Table 6: Parameters for the electronically excited system from [14].

The reason was to check whether the script would return consistent results relative to previous research described in [14], where electronically excited states in similar structures were investigated. As can be seen in figure 9 the program has been validated for this situation.

3.7 Trapping

To include the trapping of the excitation at the N^{th} site the last diagonal element of the Hamiltonian was changed to

$$H_{NN} = -Cx_N + i\Gamma. \tag{70}$$

When inserted into the time evolution operator (9) the population located at the N^{th} site gets multiplied by constant smaller than 1 since the exponent in the time evolution operator is also complex. This causes the total population to decay over time. The decay generally has the form displayed in figure 10.

The reason that the population harvesting shows this particular form has to do with the fact that the exciton is initially localized at the first site, therefore the total population starts of at one. Since the particle is localized at the first site it takes a while for the harvesting to take place since the intersite coupling decreases with $\frac{1}{|n-m|^3}$, therefore the population that immediately transfers to the last site is very small. As time moves on though the exciton will localize at sites closer to the trap and the harvesting rate picks up considerably.

4 Results

4.1 Cluster

A large amount of iterations is required to remove some of the randomness of the harvesting time. The amount of time that the coupled system has to

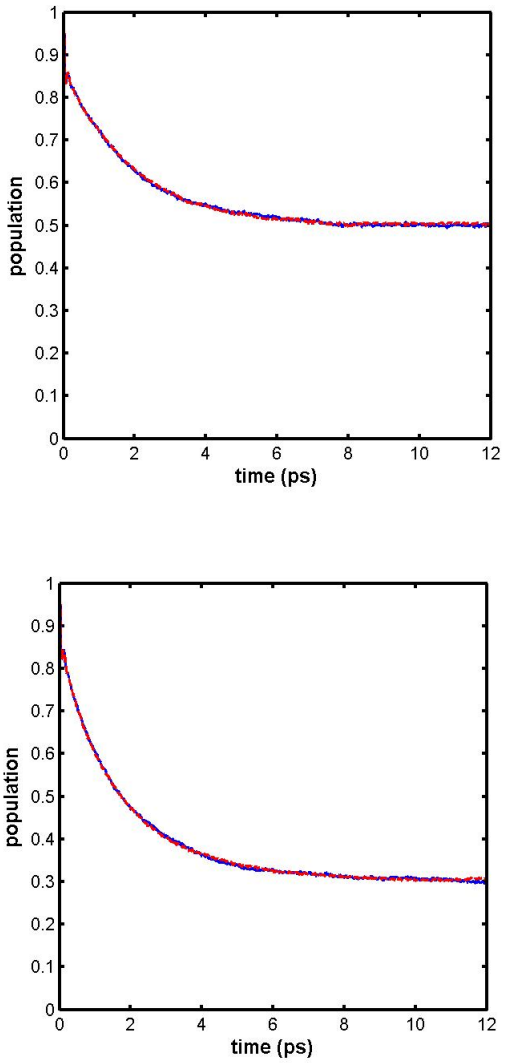

Figure 9: Simulations were run for a dimer with the parameters displayed in table 6, for the sake of validation of the currently used scripts. The dashed red lines represents the previous program over 10000 iterations, the solid blue lines represent the current program run over 6000 iterations. The y-axis represents localization on the high energy site and the x-axis displays the time in ps. The first image includes coupling of the classical system to the quantum system. The second image contains both coupling of the classical system to the quantum system as well as feedback from the quantum system to the classical system.

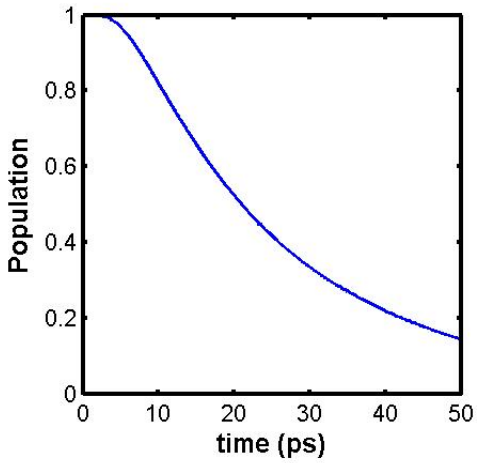

Figure 10: The total population ($< \psi|\psi >$) as a function of time. $\Delta = 300$, $C = 5000$ and the chain has a total of 25 sites.

be propagated over before most of the energy has been trapped is significant. Since it is desirable to evaluate a polymer chain of at least 20 sites rather large computational times are required. Therefore the experiments have been run parallel on the Millipede computer cluster.

4.2 Dimer

As an intermediate step simulations have been run with a dimer ($N = 2$) rather than a molecular chain. The reason for this is that matrix multiplications with a two dimensional matrix are significantly less computationally expensive than matrix multiplications involving 25-dimensional matrices. An initial result for the choice of quantum parameters: $\Delta = 300$ and $C \in [0, 5000]$ lead to the result of figure 11.

Even at 500 iterations the randomness in the result is still clearly visible. To clarify the result, a third order least squares polynomial was determined and plotted alongside the results. The minimum is approximately located at $C = 4000$. Surprisingly the Stokes shift is not near Δ, since inserting $C = 4000$ and $k = 274$ into (20) leads to $|\Delta\omega| = 701\ cm^{-1}$. Remembering the image displaying the the role of the Stokes shift to the energy levels, this would imply that the minimum harvesting time is located at a position were the energy level of the initial site falls below the energy level of the following site.

A similar image was made for the the set $J = 3700$, $\Delta \in [0, 500]$, see figure 12. It should be noted that the least squares graphs are consistent at the intersection point. To obtain a clear image of the interdependency of the intersystem

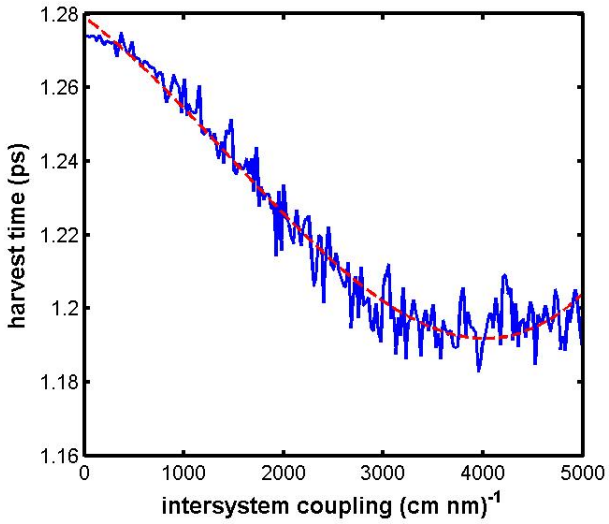

Figure 11: The blue solid line represents the harvesting time in ps as a function of C in $(\text{cm nm})^{-1}$ for a dimer with $\Delta = 300$. The red dashed line is a third order least squares polynomial through the blue line. At every data point and ensemble average over 500 trajectories was taken.

coupling and the bias, simulations were run on each of the grid points. The used grid was of the form demonstrated in figure 13. At each point 500 trajectories were calculated and the found harvesting time was averaged over. This led to figure 14. For some grid points the simulations returned inconclusive results, as there were relatively few of these points they were corrected for by setting them equal to their nearest neighbour on the C-line. A more smooth graph was made by finding a least squares approximation for every horizontal grid line. The result is displayed in figure 15. The result of figure 14 can be made more clear by finding the minima on every horizontal line. This is shown in figure 16. The blue solid line in figure 16 is determined by finding a third order least squares approximation of the location of the minima for every horizontal line. This means that there is in fact a minimum in the origin it just means that for all values of Δ smaller than 50 cm^{-1} the harvesting time is never smaller than for a coupling equal to zero.

Alternatively a graph can be made that displays the location of the optimal bias for a given coupling rather than the other way around, this is shown in figure 17.

A few other things should be noticed. For roughly the first 50 wave numbers of Δ the harvesting time is a monotonically increasing function of the coupling. Similarly for the intersystem coupling, at the first 200 $(\text{nm cm})^{-1}$ having a bias of zero produces optimal harvesting times. The physical interpretation for the points where the stokes shift exceeds the minimum line is that the Stokes shift

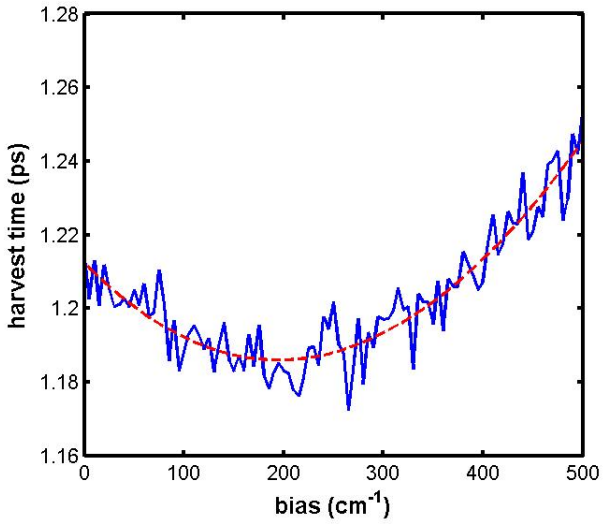

Figure 12: The harvesting time in ps as a function of the bias Δ in (cm^{-1}) for a dimer. The blue solid line displays the found data, the red dashed line represents a third order least squares fit.

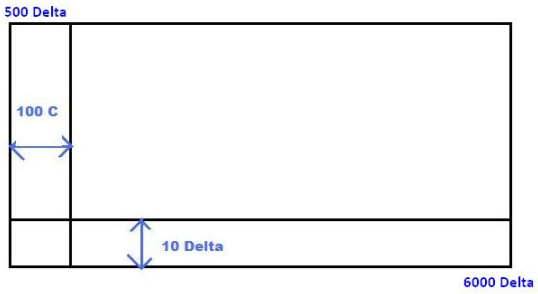

Figure 13: A graphical display of the grid containing the data points where the harvesting time of a dimer was evaluated.

is causing the energy level of the initial site to fall below the energy level of the neighbouring site. This should mean that the only way the exciton can propagate is if the heat bath randomly supplies a suitable amount of energy.

The points on the line for which it was found that the Stokes shift exceeds the the optimal bias can be explained by the localization that is lost via the inter site coupling. The harmonic oscillator coupled to the first site has a correlation time that is longer than the timescale of the timestep, therefore some of the population has leaked away from the first site before the Stokes shift has fully set in. This causes the site to feel a smaller effective Stokes shift, hence a smaller

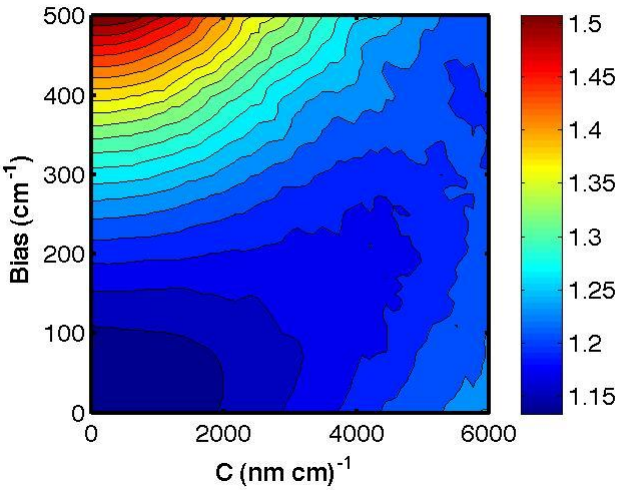

Figure 14: The returned harvesting time at each grid point (see figure 13). The color corresponds to the harvesting time in ps, every grid point was averaged over 500 iterations.

bias causes resonance between the sites.

4.3 Polymer

Similar investigations were performed for a polymer chain of 25 sites. Due to the aforementioned computational limitations a significantly rougher grid was evaluated. The evaluated grid was of the form displayed in figure 18

The found result is of the form displayed in the surface plot of figure 19

A few noticeable features become apparent. The value of the harvesting time cannot exceed 50 ps, the reason for this follows from the definition of the harvesting time in (68) that the maximum possible harvesting that can be calculated over an interval of 50 picoseconds is also 50 picoseconds. It also means that from these points no noticeable harvesting occurs. This is of course not an accurate measurement but since we are only interested in the minima it is of no consequence. The dependence on the coupling wasnt properly visible so an extra two rows were added to the grid, one row located at $\Delta = 25\text{cm}^{-1}$ and another row at $\Delta = 75\text{cm}^{-1}$. The plot displayed in figure 20 displays the found minimum line.

As can be seen the discrepancy found in the dimer only becomes more exacerbated for larger chains. Physically it is very easy to imagine why the given explanation for a dimer only has a greater effect for larger systems. Firstly there are more sites pulling at the exciton, therefore a greater population leaks away from a site before the correlation time has passed. Secondly and more impor-

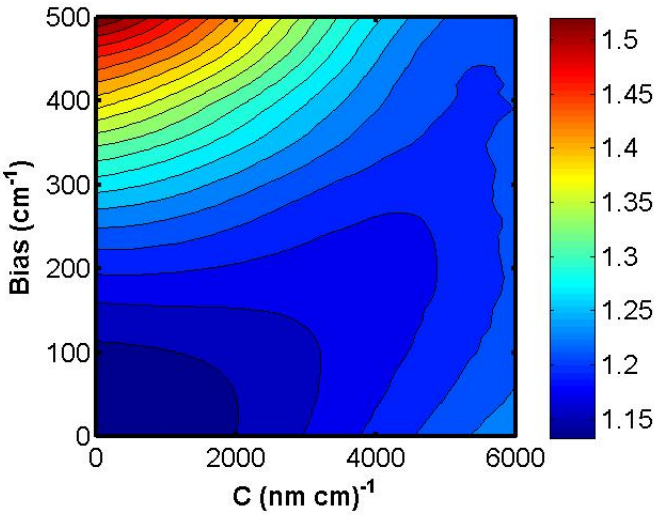

Figure 15: The same graph as figure 14 only featuring third order least square approximations along the horizontal grid lines.

tantly more sites means the exciton has to pass more sites before reaching the reaction center. This last one means that at every site the exciton will spread out more and more over the chain and smaller biases are necessary to maximize the amount resonance between the energy levels.

4.4 Graphical user interface

For the sake of ease of use and for demonstrational purposes, a Graphical User Interface (GUI) was constructed using Matlab. This GUI provides the display depicted in figure 21.

The different applications can be selected from the drop down menu. The default option Classical will generate positions as a function of time of a harmonic oscillator coupled to a Gaussian heat bath. The plotted data is found by applying the Verlet-BFD scheme to equation (13). Note that for this option there is no coupling to the quantum subsystem, for this option see the setting classical (fb). The initial conditions are set as

$$x(0) = 0,$$
$$x(dt) = dt.$$

The menu option labeled Quantum will return the population located at the

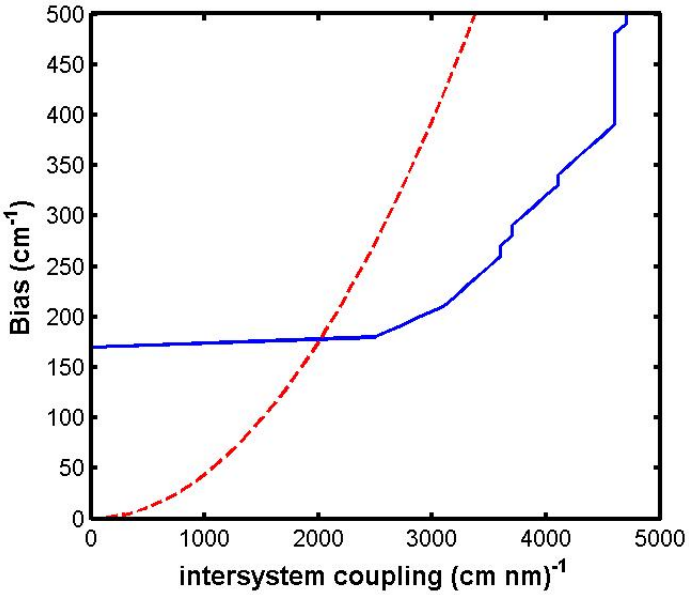

Figure 16: The horizontal minima of figure 14, figure the x-axis depicts C in $(cmnm)^{-1}$ the y axis represents Δ in cm^{-1}. The red dashed line represents the theoretical minimum, the blue line represents a second order least square fit of the actual minima. Every point on the blue line represents a minimum on its respective C-line.

first site as a function of time, for a chain with the selected parameters, but the harvesting process will not be included, i.e. the total population will stay constant in time.

The option Harvesting will display the total population as a function of time in the case that the population is harvested from the last site.

Finally the option 'classical fb' as before shows the position of a classical oscillator as a function of time but this one is coupled to the quantum subsystem. As a consequence it can be used to view the Stokes shift. The reason for which this function is separate from the option classical has to do with the nature of the initial conditions. Just like in the actual simulation the initial conditions were found by letting the system integrate off-screen for an amount of time equal to the given final time, the initial positions of this interval were both set equal to zero. The last two points of this initial integral are set to be the first two positions of the displayed interval. Besides that the cost increases significantly since the quantum subsystem has to be integrated in the background. Therefore it is advisable to use the option 'classical' if intersystem coupling is not required.

The parameters that can be defined by the user are described in table (7) along with the settings that are defined on start-up.

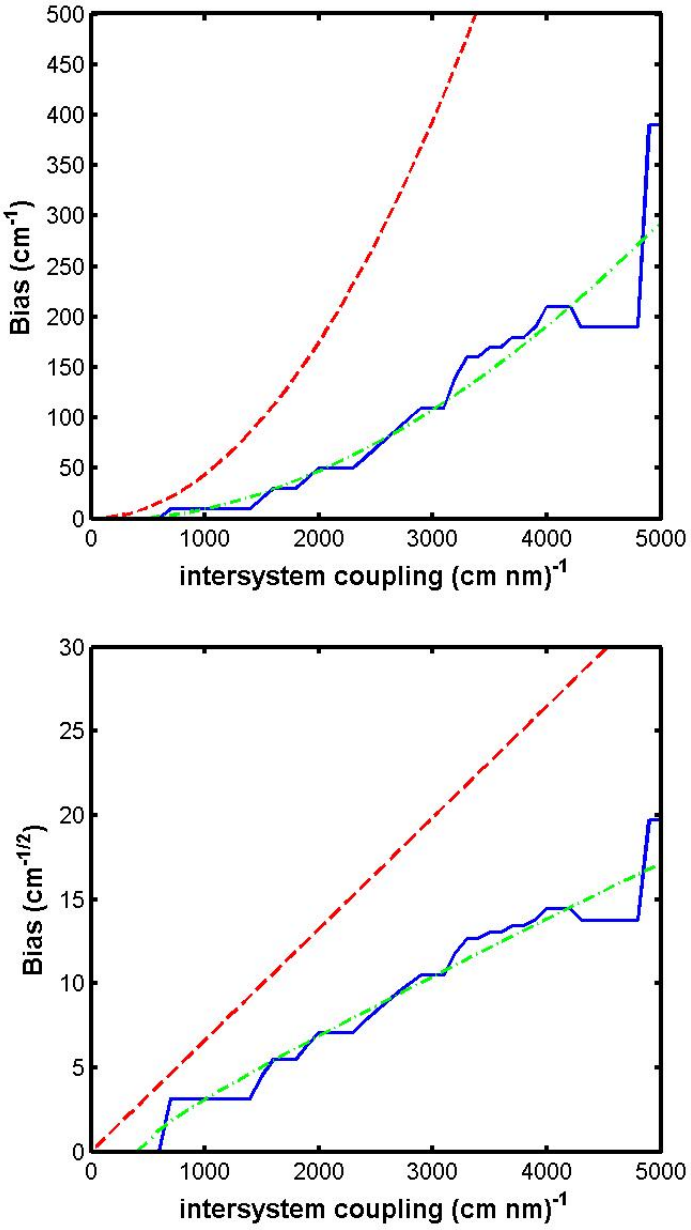

Figure 17: The first plot depicts the minima over vertical grid lines for a dimer evaluated at the grid displayed in figure 13. The blue line depicts the minima of figure 15, the red dashed line represents minimum line that would be expected due to the the Stokes shift and the green line is a third order least squares approximation of the blue line. The second plot displays the square root of the data of the first plot, hence it can be seen that the result is in fact quadratic.

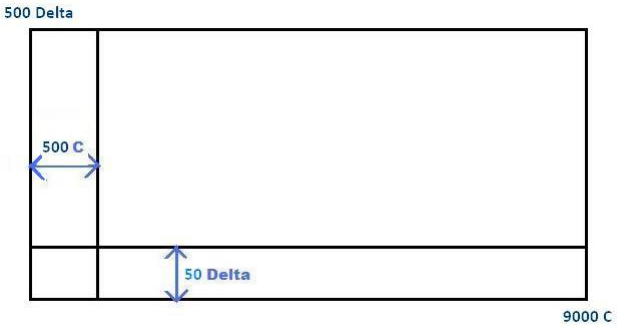

Figure 18: The grid that was used to discretize the parameter space.

Parameter	**unit**	**description**	**initial setting**
k	u*ps^{-2}	the spring constant	274
γ	ps^{-1}	the friction constant	137
m	u	the mass of the classical particle	1
Δ	cm^{-1}	the bias in the two-level systems	300
C	(cm nm)$^{-1}$	The inter system coupling	3000
J	cm^{-1}	The inter site coupling	600
dt	ps	The integration timestep	0.01
sites		The amount of sites the chain consists of	2
iterations		The amount of samples that is averaged.*	1
final time	ps	The upper integration bound**	5

Table 7: A description of the parameters that can be set in the GUI. *Only relevant when using the 'Quantum' or 'Harvesting' options. **Note that this value should be a multiple of dt.

The edit text boxes can be used to set the parameters to specific values. Alternatively for the friction and spring constant the sliders can be used. The downside of the sliders though is that the set value is not displayed on the interface itself, rather the updated values are displayed in the Matlab command window.

5 Discussion

It has been shown that with a suitable choice of parameters and choice of timestep the global error can be kept small relative to deviation caused by the inherent stochastic nature of the process. More complicated algorithms can be used such as Runge Kutta methods or the velocity-Verlet scheme but it was shown that the simple combination of the Verlet method and a finite difference method was sufficient to keep the truncation error small compared to the ran-

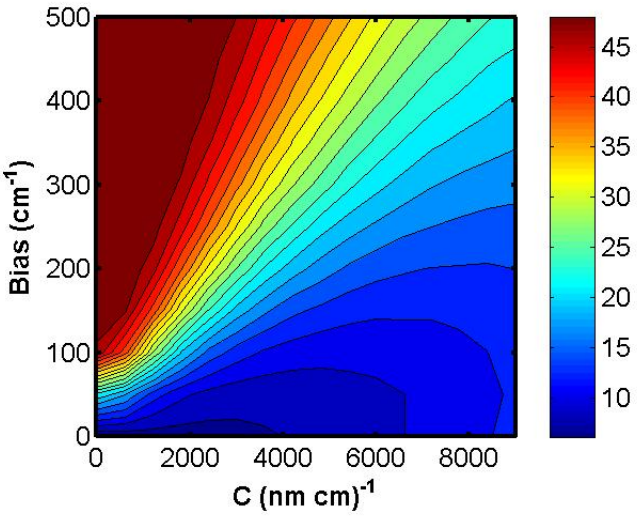

Figure 19: The harvesting time (τ_h) in ps as a function of Δ in $(\text{cm})^{-1}$ and J in $(\text{cm nm})^{-1}$ for a polymer consisting of 25 sites.

dom fluctuations. Also the Verlet-backwards finite difference method is in this case arguably better suited than the velocity-Verlet method as the former has a local error of the order $(\Delta t)^3$; compared to the $(\Delta t)^2$ order of the velocity-Verlet scheme. Of course the global error of both methods converge with second order and in the former method more care has to be taken in picking parameters.

The found line in the parameter plane where the minimum harvesting time is located is shifted away from the Stokes shift line. The expected reason for this is due to correlation time defined in (64), the chosen value was rather large and the intersite coupling is rather strong compared to the used values of Δ. Therefore a significant amount of the population located at the initial site has leaked away to the other sites before the respective mass-spring system has had the time to respond. Hence it feels a lower population than expected at each site and the Stokes shift has to greater to compensate for it.

There are still a lot of ways available to increase the accuracy of the results. The simplest way to gain better results is use a finer grid. To use a molecular chain for the main result instead of a dimer would be preferable but the time and computational limitations are quite severe as the $expm()$ function requires multiple matrix multiplications the complexity increases as n^3. Also a simple condition that would stop the simulation once the total remaining population is smaller than a certain value would have been a great addition. This would cut the computational time in half for certain faster grid points, since for certain

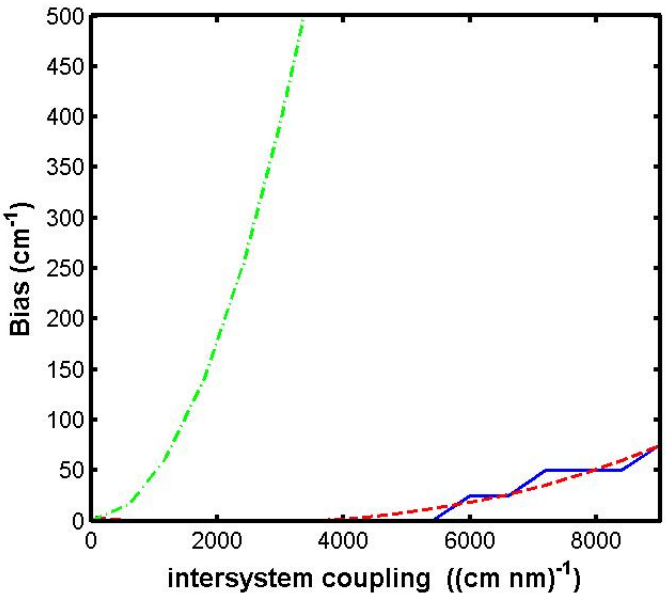

Figure 20: The blue solid line represents the found minimum in the harvesting time for polymer consisting of 25 sites. The pink dashed line is a third order least squares polynomial through the minimum line. The green dash-dot line represents the minimum line that would be expected based on the Stokes shift.

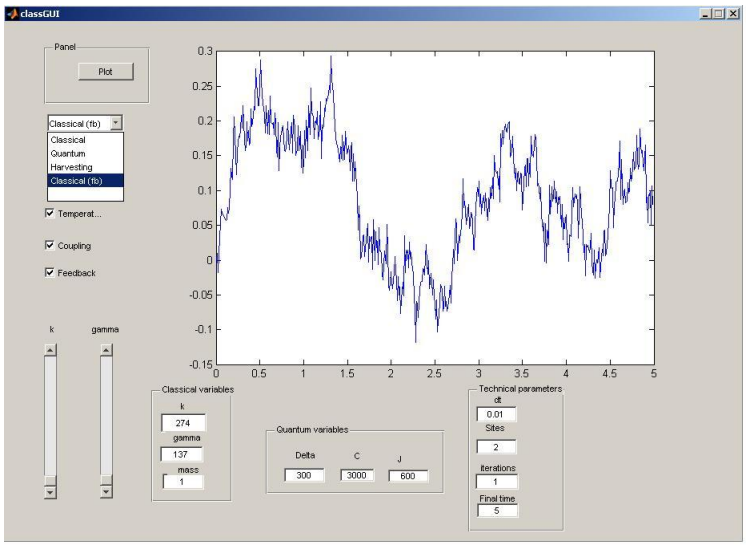

Figure 21: The GUI in use.

Improvement	Cost increase
More site	Cubic
Finer Grid	Linear\Quadratic
Larger time intervals	Linear
More trajectories	Linear

Table 8: The speed at which the cost increases as certain improvements to the experiment are added.

choices of parameters the population has almost been fully harvested at half the final time. It would also mean that the maximum allowed number of timesteps could be increased such that more accurate results could be found for the slower grid points. Another way to increase the accuracy would be to increase sample size of the ensemble average. All results were obtained after averaging over 500 trajectories but as can be seen in figure 9 this hardly even begins to completely remove the inherent randomness of the process. But of course the complexity increases linearly with the amount of required iterations.

Of course any improvements to the result will significantly increase the cost. This is summarized in table 8

6 Conclusion

The goal of this thesis has been to evaluate the transport properties of a general chain-like light harvesting system. To do this the degrees of freedom of the system were separated into molecular coordinates and electronic coordinates.

Each of these coordinates were evaluated using two different models which were allowed to interact with each other. The electronic coordinates were modeled as electronically coupled quantum mechanical two-level systems. The larger scale molecular coordinates were approximated using classical dynamics. This was done by considering it to be a harmonic oscillator coupled to a Gaussian heat bath.

The resulting feedback system was numerically integrated. To integrate the quantum subsystem Numerical Integration of the Schrödinger Equation (NISE) method was applied. To integrate the classical subsystem a variation of the Verlet integration scheme was applied. A sufficient but not necessary stability condition was found such that this scheme could be integrated without large deviations due to truncation error propagation.

The NISE method was used to evaluate the quantum system. This required that the time evolution operator is constructed at every timestep. For this purpose Matlabs $expm()$ function was used. This caused the complexity of the total algorithm to become exceedingly large for longer structures. It was demonstrated that the complexity increases with n^3, where n represents the amount of sites.

It was hypothesized that the Stokes shift would cause the harvesting process to accelerate if a bias were to be present in the chain. For a dimer it was found to be the case that a bias can indeed have an enhancing effect to the harvesting time. The found dependence on the intersystem coupling revealed that the dependence on the Stokes shift isnt as trivial as expected. The result still appears to be quadratic and order of magnitude is not far off, therefore the hypothesis is likely not entirely wrong. The deviance was explained to be due to the delay in the classical system, it takes a while for the the excited classical particle to relax back into it's equilibrium position. During this process the minimum in the potential shifts back to zero as the exciton leaks away from it's position. This leads to a smaller required bias to cause resonance between neighboring sites.

For a polymer chain it can still be found that a bias can have an augmenting effect towards the harvesting time, but it was also shown that an exceedingly large intersystem coupling is required before a noticeable effect can occur.

Previous models as in [9] have modeled the disorder in the chain as a static Gaussian disorder in the energy levels. This model deviates from those by assuming dynamic dynamic energy levels, which are calculated alongside the propagation of the exciton. These models show that for small chains a relatively large bias can possibly accelerate the harvesting time. Larger systems on the other hand will generally not benefit from large biases.

6.1 Acknowledgments

I am grateful for the time and help provided by: Thomas Jansen; Bruno Carpentieri; Niels van der Vegte and the rest of the theory of condensed matter group at the Zernike Institute of Advanced Materials, Groningen

References

[1] Valeur B.; *Molecular Fluorescence, Principles and Applications*,Wiley-VCH,2002

[2] Schulten K.; available: http://www.ks.uiuc.edu/Research/psures/ [2012, Juli 5]

[3] Jansen T.l.C.; Knoester J. *Journal of Physical Chemistry*, **2006**, 110, 22910-22916

[4] Vlaming S.M.; Malyshev V.A. *Journal of Physical Chemistry*, **2007**, 127, 154719

[5] Harel, E *Journal of Physical Chemistry*, **2012**, 136, 174107

[6] Jansen T.l.C.; Knoester J. *Journal of Physical Chemistry*, **2007**, 127, 234502

[7] Olbrich C.; Jansen T.l.C.; Liebers J.; Aghtar M.; Strümpfer J.; Schulten K.; Knoester J.; Kleinekathöfer U. *Journal of Physical Chemistry B*, **2011**, 115, 8609-8621

[8] Damjanovic A.; Kosztin I.; Kleinekathöfer U.; Schulten K.; *Physical Review E*, **2002**, 65, 031919

[9] Vlaming S.M.; Malyshev V.A.; Knoester J. *Elsevier Journal of Luminescence*, **2008**, 128, 956-959

[10] Jansen T.l.C.; Knoester J. *Accounts of Chemical Research*, **2009**, 42(9), 1405-1411

[11] Verlet L.; *Physical review*, 1967, 159, 98-103

[12] Lust K; Verstappen R.W.C.P.; *Reader COPO course, Rijksuniversiteit Groningen, p196,* ***2010***

[13] Higham N.J.; *SIAM Journal on Matrix Analysis and Applications*, **2005**, 26(4), 1179-1193

[14] van der Vegte, C.P.N.; unpublished manuscript, Rijksuniversiteit Groningen

[15] Burder R.L.; Douglas Faires J.; *Numerical Analysis*, 9th ed., Brooks/Cole **2011**

[16] Hairer E.; Lubich C.; Wanner G.; *Acta numerica*, **2003**, 12, 399-450

[17] Liboff R.L.; *Introductory Quantum Mechanics*, 4th ed., Pearson education, **2002**

[18] MATLAB © *2012 The MathWorks, Inc. MATLAB and Simulink are registered trademarks of The MathWorks, Inc. See www.mathworks.com/trademarks for a list of additional trademarks. Other product or brand names may be trademarks or registered trademarks of their respective holders.*

[19] Quarteroni A.; Sacco R.; Saleri F.; *Numerical Mathematics, Text in Applied Mathematics*, 2^{nd} edition, Springer, **2006**